Dentomaxillofacial Radiology (2015) 44, 20140238

birpublications.org/dmfr

CBCT SPECIAL ISSUE: REVIEW ARTICLE

CBCT-based bone quality assessment: are Hounsfield units applicable?

[1,2]R Pauwels, [2]R Jacobs, [3]S R Singer and [4]M Mupparapu

[1]*Department of Radiology, Faculty of Dentistry, Chulalongkorn University, Bangkok, Thailand;* [2]*OMFS-IMPATH Research Group, Department of Imaging and Pathology, Faculty of Medicine, Catholic University of Leuven, Leuven, Belgium;* [3]*Division of Oral and Maxillofacial Radiology, Department of Diagnostic Sciences, Rutgers School of Dental Medicine, Newark, NJ, USA;* [4]*Division of Radiology, Department of Oral Medicine, University of Pennsylvania School of Dental Medicine, Philadelphia, PA, USA*

CBCT is a widely applied imaging modality in dentistry. It enables the visualization of high-contrast structures of the oral region (bone, teeth, air cavities) at a high resolution. CBCT is now commonly used for the assessment of bone quality, primarily for pre-operative implant planning. Traditionally, bone quality parameters and classifications were primarily based on bone density, which could be estimated through the use of Hounsfield units derived from multidetector CT (MDCT) data sets. However, there are crucial differences between MDCT and CBCT, which complicates the use of quantitative gray values (GVs) for the latter. From experimental as well as clinical research, it can be seen that great variability of GVs can exist on CBCT images owing to various reasons that are inherently associated with this technique (*i.e.* the limited field size, relatively high amount of scattered radiation and limitations of currently applied reconstruction algorithms). Although attempts have been made to correct for GV variability, it can be postulated that the quantitative use of GVs in CBCT should be generally avoided at this time. In addition, recent research and clinical findings have shifted the paradigm of bone quality from a density-based analysis to a structural evaluation of the bone. The ever-improving image quality of CBCT allows it to display trabecular bone patterns, indicating that it may be possible to apply structural analysis methods that are commonly used in micro-CT and histology.
Dentomaxillofacial Radiology (2015) **44**, 20140238. doi: 10.1259/dmfr.20140238

Cite this article as: Pauwels R, Jacobs R, Singer SR, Mupparapu M. CBCT-based bone quality assessment: are Hounsfield units applicable?. *Dentomaxillofac Radiol* 2015; **44**: 20140238.

Keywords: cone-beam computed tomography; Hounsfield units; bone quality; dental implants

Introduction

The introduction of CT devices in the early 1970s led to an eventual discourse on the quantification of anatomical structures, especially calcified structures such as the bone and teeth. Multidetector CT (MDCT) devices used advanced computational functions to derive images of high spatial and temporal resolution and also specific density values that are termed Hounsfield units. The introduction of CBCT has allowed clinicians to view the craniofacial structures in three dimensions at a relatively high spatial resolution, which has led to a more widespread use of three-dimensional (3D) imaging in dentistry in recent years. Although clinicians are using gray values (GVs) derived from CBCT units, it is not certain that the grey shades are consistently representative of the actual density values, and even further, it is not certain if they are similar to the Hounsfield units that are derived from medical CT scanners. The purpose of this manuscript is to investigate, via a critical review, the applicability of Hounsfield units in CBCT-derived density measurements. In the first section, current concepts related to the evaluation of bone for implant placement are discussed. Next, the reliability and applicability of quantitative

Correspondence to: Dr Ruben Pauwels. E-mail: pauwelsruben@hotmail.com
Received 9 July 2014; revised 2 October 2014; accepted 13 October 2014

GVs in CBCT are reviewed. Finally, a brief overview of alternative methods for bone analysis, independent of numerical GVs, is given.

Evaluation of bone for implant placement: current state

Over the past 30 years, oral implant placement has evolved towards a predictable and routine treatment option, with reported success rates exceeding 95%.[1,2] There are many variables and clinical conditions reported to have some potential influence on implant success, including local and systematic disease condition, smoking habits, intravenous medications interacting with bone metabolism and radiotherapy.[3] Considering that all these variables and conditions may directly or indirectly affect bone conditions, it is obvious that attention should be paid to the local bone quantity and quality during the pre-surgical planning phase.

Bone quality: essential but ambiguous

Bone quantity can be defined as the amount of bone height and the width of the alveolar crest at an edentulous site. The term "atrophy" is used to denote the amount of loss of normal alveolar bone secondary to the loss of a tooth. The term "bone quality", however, is not so simple to define. There is no clear consensus on the definition of bone quality, but, in general, it encompasses multiple aspects of bone physiology, the degree of mineralization, the morphology and type of trabecular pattern.

Bone quality has been suggested as one of the main factors influencing implant therapy success. Areas of lesser bone quality have exhibited higher failure rates and weaker primary stability values.[4,5] Quality of cortical as well as cancellous bone may affect primary implant stability and therefore success of treatment.[6,7]

In poor bone quality areas, the implant failure rate tends to be higher, because implants depend on the surrounding bone for their support and retention.[8] By contrast, in areas of good bone quality, such as the anterior mandible, implant success rates may be correspondingly higher.[2] It should be kept in mind that implant failure has been shown to be closely related to local bone characteristics and previous inflammation (such as a chronic apical inflammatory lesion resulting in a local osteosclerotic scar or a remnant osteolytic lesion).[9] Another factor of importance may be intravenously administered bisphosphonates. Indeed, Marx[10] indicated that bisphosphonates prevent renewal of old and injured bone, thus making it brittle and more prone to fracture. Furthermore, Marx demonstrated that bisphosphonates have a 11-year half-life in the bone because of the irreversible binding to the bone via a central carbon atom. In addition, when administered intravenously, bisphosphonates accumulate 143-times faster in the bone than when administered orally. Intravenous use in Wistar rats did not seem to interfere with osseointegration, but a possible lack of bone remodelling of the original cortical bone may affect long-term osseointegration,[11] while topical administration might even positively affect implant survival in the pre-loading and post-loading phases in partially and fully edentulous patients.[12]

From the aforementioned evidence, bone quality assessment should be strongly recommended during the pre-surgical implant-planning phase. What usually exists are peri- or post-surgical methods to test implant stability, during or after placement (measurement of bone stiffness, damping characteristics, resonance frequency).[13–15] Yet, such methods come too late for deselecting unfavourable implant sites. Furthermore, some pre-operative methods, such as ultrasound bone quality assessment, are not readily available in dental practice and are poorly understood in oral implant surgery.[15]

Use of radiography for evaluation of bone quality

Radiological bone quality evaluation should be an essential element of pre-surgical implant planning, as it is a widely available and relatively non-invasive method to assess bone quality of the jaws. One may initially think of intraoral and panoramic radiographs, considering their wide availability in oral healthcare; however, the inherent 3D nature of the surgical site has moved pre-surgical planning towards the use of dental CBCT, as it can offer high-quality 3D images at relatively low radiation doses and costs. Apart from the radiodiagnostic possibilities, dental CBCT may offer perisurgical potential (*e.g.* surgical navigation and drill guides), explaining part of the success of CBCT for oral implant placement. The latter implies that one has also to focus on potential techniques for bone quality assessment using clinical CBCT data sets.

In practice, implant surgeons may have difficulty in radiographically determining the pre-operative quality of cancellous bone available for proper implant support. The use of subjective radiological rating scales has been proposed to provide a pre-operative assessment of bone quality, as evidence demonstrates a relationship between poor bone quality and increased implant failure rate.[6,16–18] Most grading scales are based on the characterization of cross-sectional trabecular morphology[19] and cortical bone thickness.[20,21] Yet, there is no single universally accepted system for classifying bone quality in the maxilla and mandible.[15,22,23] The most traditional method applied during pre-operative implant assessment is that of Lekholm and Zarb,[24] categorizing bone quality into four groups according to the degree of cortication and trabecular bone morphology. This classification system is based on the premise that successful osseointegration coincides with greater cortical density and smaller trabecular spaces. This assertion has been supported by a number of older studies and may hold true when dealing with the classical "machined" implant surface.[6,16–18] It should be considered that with the introduction of new and improved implant surface characteristics, this effect has surely weakened.[25] These changes to the manufacturing of implants have tremendously changed the requirements of bone quality. What is

currently considered necessary for successful osseointegration is a healthy and well-vascularized bone. This is further discussed in the last section of this review.

Hounsfield units

When evaluating or classifying the density of the bone, GVs obtained from 3D CT images are quantified as Hounsfield units. This implies that for every image voxel, a Hounsfield unit value based on the material inside that voxel needs to be determined during image reconstruction. Hounsfield units are defined as linear transformations of measured X-ray attenuation coefficients of a material with reference to water. Hounsfield units can be calculated for any material using the formula:

$$HU_{material} = 1000 \times \frac{\mu_{material} - \mu_{water}}{\mu_{water}}$$

wherein $\mu_{material}$ and μ_{water} are the linear attenuation coefficients for the material and water, respectively. The Hounsfield unit scale is based on two fixed values, which are 0 HU for water and −1000 HU for air ($\mu_{air} = 0$). Materials or tissues that absorb more X-rays, such as bone, have a higher Hounsfield unit value. Although Hounsfield unit values are not absolute measurements of material density, they can be used for clinical purposes to quantify bone material density (BMD). Although Hounsfield units can be converted to BMD, it is possible to derive BMD from attenuation coefficients without the need for Hounsfield unit calibration. This is carried out through the use of BMD phantoms, which contain at least two materials of varying density. When BMD calibration is performed in CT, the procedure is referred to as quantitative CT (qCT). Currently, qCT is commonly applied for the detection and follow up of osteoporosis through analysis of BMD in the lumbar spine, hip and limbs. It can be considered as an alternative to dual-energy X-ray absorptiometry, yielding more accurate BMD estimations for specific groups (*e.g.* arthritic, scoliotic or obese patients). BMD calibration is also performed in micro-CT (μCT) for research purposes (*e.g.* animal specimens) or for the analysis of extracted human bone samples.

In dentistry, Hounsfield units have been applied for the determination of the quality of bone at the site of implant placement, as it would lead to a more accurate prognosis of the impending osseointegration. Although Hounsfield units still have a potential role in bone quality assessment, their relevance has been questioned owing to recent evolutions in implant dentistry to go beyond the evaluation of bone density. This is further discussed in the last section of this review; first, the applicability of Hounsfield units in CBCT will be reviewed in detail.

Applicability of Hounsfield units in CBCT

The use of bone density measurements using CBCT for clinical applications is a precise task, requiring high stability and reliability of GVs and a consistent correlation between GV and density. Various issues are associated with the use of Hounsfield unit values in CBCT. These issues relate to the limited-field CBCT geometry, basic radiation physics principles and the assumptions and limitations of currently used reconstruction algorithms. The following types of GV inaccuracies exist:

- Variability in the axial plane. This can vary from cupping and doming artefacts, beam hardening, to shading induced by mass outside the field of view (FOV).
- Variability between axial slices (*i.e.* along the *z*-axis) owing to varying mass per slice (*i.e.* various degrees of the above effects) and divergence of the X-ray beam (when not corrected during reconstruction).
- High image noise. Owing to the random nature of noise, it does not affect the mean GV, especially when evaluating large regions. For small regions of interest, noise may have a minor effect on the mean GV.

It should be noted that, in current CBCT imaging, several manufacturers do not attempt to calibrate GV along a (pseudo-) Hounsfield unit scale, which can be considered an acknowledgement of GV inaccuracy rather than an inherent limitation of CBCT.

For further information on the technical and reconstruction principles of CBCT and various types of artefacts interfering with GV accuracy, we kindly refer you to other works.[26–28] The remainder of this section will focus on experimental findings related to the accuracy and clinical application of GV in CBCT. Studies on non-dental CBCTs will not be discussed, although the inherent issues and findings are similar,[29,30] and corrections have been proposed that may be applicable for dental CBCT as well.[31–33]

Literature review: accuracy and stability of gray value in CBCT

Table 1 provides an overview of selected studies in which the accuracy/potential application of CBCT GV is evaluated. Results from each study are briefly described. In some cases, additional analyses were made, for example, correlation coefficients were calculated based on GVs provided in the article, or GV errors were calculated or derived from plots.

In general, each study in Table 1 provides information illustrating the various issues related to CBCT GV described in the above section. In several cases, the authors may have been too optimistic in the interpretation of the results, claiming that Hounsfield units can be applied in CBCT despite the fact that their study, like most others, shows large potential GV errors. Most often, too much reliance is put in the value of a correlation coefficient, which is a limited metric prone to subjective interpretation. In some cases, possible GV corrections are proposed with generally promising results, although they are typically *ad hoc* (*i.e.* applicable only on the data and CBCT model used in that study).

Table 1 Studies evaluating the accuracy and stability of gray values (GVs) in CBCT

Study	*CBCT models*	*Phantom*	*Materials*	*Reference*	*Results*[a]
Aranyarachkul et al[34]	1	Human cadavers ($n = 9$)	Bone	Quantitative CT	$R^2 = 0.85$–0.96
Azeredo et al[35]	3	Small cubic phantoms	Air, water, wax, acrylic, plaster, gutta-percha	CT	$R^2 = 0.8818$–0.9947 (average, 0.9370)
Bamba et al[36]	3	Cylindrical PMMA phantom	Air, LDPE, PMMA, POM, PTFE, aluminium	CT	Uniformity in axial and coronal plane: variable results, shifts of >1000 GV for one CBCT model Effect of scan parameters (kVp, mAs) and environment (amount of PMMA) demonstrated
Bryant et al[37]	1	Assymetric acrylic phantom Terraced phantom Pyramid phantom Water phantom	Acrylic Water	N/A Theoretical Hounsfield units (*i.e.* 0 HU)	GVs affected by mass in slice and mass outside slice. Stable region of 11 cm in centre of FOV Correction equation proposed based on mass of 7 g per slice
Bujtár et al[38]	1	Cadaver head	PE, POM, borosilicate glass, aluminium, water	CT	Effect of position: SD, 70–135 (maximum shift, 193–488 GV) CBCT-CT: R^2, 0.82–0.98
Cassetta et al[39]	1	Mandibles ($n = 10$)	Cortical and cancellous bone	N/A	Effect of mAs (approximately 47% reduction): cortical bone: shift of 161 GV cancellous bone: shift of 65 GV
Cassetta et al[40]	1	Mandibles ($n = 20$)	Cortical and cancellous bone	CT	$R^2 = 0.87$–0.96 (average, 0.93) Average difference between CBCT and CT, 235 GV
Chindasombatjaroen et al[41]	1	Cylindrical water phantom	Iodine contrast medium 0.0625–8%, concentration doubled with each step	CT	$R^2 = 0.9997$–0.9999 Effect of mAs: GV shifts up to approximately 150 GV (Effect of kVp also demonstrated)
Eskandarloo et al[42]	3	Rectangular phantom filled with water and oil	PE, polyamide, PVC, bone pieces	CT	Effect of position in FOV: Model 1: average shift, 125 GV; maximum, 291 GV Model 2: average shift, 39 GV; maximum, 141 GV Model 3: average shift, 106 GV; maximum, 395 GV
Hohlweg-Majert et al[43]	1	Cylindrical phantom	HA (100, 200, 400, 1000 mg cm^{-3})	CT	Differences between axial slices: average shift, 24 GV; maximum, 67 GV
Katsumata et al[44]	2	Cylindrical plastic, filled with water, dry mandible and cervical vertebrae	Bone, water	CT	Difference in GV of water at buccal and lingual sides GVs and lingual-buccal differences affected by objects outside the FOV Objects outside the FOV lead to GV shifts of up to 10% of the gray scale Relative densities (normalized to bone) also not stable
Katsumata et al[45]	1	Cylindrical plastic, filled with water, dry mandible and cervical vertebrae	Bone, water	N/A	Highest variability for smallest FOV, decreased variability for larger FOVs GVs severely inconsistent between FOVs (difference of 374 GV for bone) Shifts due to objects outside FOV, 10–74 GV
Lagravère et al[46]	1	PMMA box filled with water	POM, acrylic, nylon, cork, celfortic pink foam, spruce	Physical density	Correlation between density and Hounsfield units: $R^2 = 0.986$ Standard error of 27 HU
Lagravère et al[47]	1	PMMA box filled with water	Canadian spruce, nylon, POM	Physical density	Shifts in GV due to object location up to 85–214 GV (not statistically significant) Correlation between density and Hounsfield units: $R^2 = 0.893$
Mah et al[48]	11	Small cylindrical phantom (in air and in	(Air), adipose, water, PMMA, muscle,	Linear attenuation coefficients	Highest correlation at effective beam energy

(Continued)

Table 1 (Continued)

Study	*CBCT models*	*Phantom*	*Materials*	*Reference*	*Results*[a]
		small/large water containers)	cancellous bone, cortical bone, aluminium		Hounsfield units derived through attenuation coefficients Variability in CBCT-derived Hounsfield units when scanning in air *vs* small or large water container: average shift 127 HU; maximum 1258 HU Large differences in derived Hounsfield units between CBCTs
Molteni[28]	2	Small cylindrical phantom (in air and in small/large water containers);	(Air), adipose, water, PMMA, muscle, cancellous bone, cortical bone, aluminium	Linear attenuation coefficients	Less artefacts for small FOVs Increase in GV towards the top of FOV for one CBCT model No influence of resolution mode on GV for one CBCT model Effect of exo-mass, presence of water and central/peripheral phantom position Discrepancy between central and peripheral gray values for water: −135 to +125 GV Correlation between attenuation coefficients and CBCT GV: R^2, 0.935–0.973
Nackaerts et al[49]	5	Rectangular bone mineral phantom	Water, HA (75, 150 mg cm^{-3})	CT	Poor stability of CBCT GV throughout FOV (CV, 10%; CT, 0.1%) Large effect of rotation and off-centre positioning of phantom Correlation of CBCT-CT: R^2 = 0.095–1.000 (average, 0.764; median, 0.969)
Naitoh et al[50]	1	Patients (n = 16)	Mandibular cancellous bone	CT (BMD)	Correlation CBCT GV and CT-derived BMD: R^2 = 0.931 BMD from CBCT deviates 1–182 mg cm^{-3} (average, 46 mg cm^{-3}) from CT Deviations of up to approximately 200 GV
Naitoh et al[51]	1	Patients (n = 15) Reference bone block	Mandibular cancellous bone HA (200 mg cm^{-3})	CT (BMD)	BMD from CBCT deviates 1–123 mg cm^{-3} (average, 38 mg cm^{-3}) from CT 84% of bone sites correctly classified as > or <200 mg cm^{-3} using reference block 38% in 150–250 mg cm^{-3} range misclassified
Nishino et al[52]	1	Cylindrical phantom	Air, LDPE, acrylic, PTFE	N/A	Effect of relative z-position of phantom: maximum shift, 19–69 GV (depending on material)
Nomura et al[53]	1	Water phantom	Aluminium, iodine solutions (0–100 mgI ml^{-1}, 10 mgI ml^{-1} step size)	CT	Differences due to kVp or mA variation: up to approximately 12 GV CV: CBCT, 3.7–7.8%; CT: 0.7% Linear regression, CBCT-CT: R^2 = 0.982, non-linear regression: R^2 = 0.989
Nomura et al[54]	1	Water phantom or in-air	HA (0–239 mg cm^{-3}, 40 mg cm^{-3} step size)	CT	Correlation: R^2 = 0.9983–0.9999 Large influence of air/water background Presence of hard tissue: average shift 6 GV; maximum, 9 GV Presence of metal: average shift, 15 GV; maximum, 30 GV (metal inside FOV), average shift, 13 GV; maximum, 28 GV (metal outside FOV) Variation along z-axis: SD, 8.3–10.8 GV

(Continued)

Table 1 (Continued)

Study	*CBCT models*	*Phantom*	*Materials*	*Reference*	*Results*[a]
Oliveira et al[55]	1	Water phantom	K_2HPO_4 (200–1200 ng cm^{-3}, 200 mg cm^{-3} step size)	N/A	Effect of kVp: average shift, 122 GV; maximum, 290 GV Effect of mA: average shift 40 GV; maximum, 108 GV Effect of exo-mass: average shift; 183 GV; maximum, 307 GV Effect of implant in FOV: average shift, 5 GV; maximum, 28 GV
Parsa et al[56]	1	Mandibles ($n = 10$)	Bone	CT	Correlation CBCT-CT: $R^2 = 0.937$
Parsa et al[57]	1	Mandibles ($n = 20$)	Bone	CT	Difference CBCT GV and Hounsfield units: average, 155 Correlation CBCT-CT: $R^2 = 0.794$
Parsa et al[58]	2	Mandible ($n = 1$)	Bone	N/A	Model 1: effect of FOV size: maximum shift, 402 GV effect of time 1 (resolution mode): average shift, 3 GV effect of time 2 (rotation mode): average shift, 29 GV Model 2: effect of FOV size: maximum shift, 116 GV effect of mA: average shift, 36 GV effect of exposure time: average shift, 4 GV
Pauwels et al[59]	7	Cylindrical PMMA phantom	Air, PMMA, HA (50, 100, 200 mg cm^{-3}), aluminium	CT	Correlation CBCT-CT: All materials: $R^2 = 0.6864$–0.9996 (average, 0.9689) Medium density: $R^2 = 0.7303$–0.9909 (average, 0.9156) Uniformity of GV in axial plane, 4–21%
Pauwels et al[60]	13	Cylindrical PMMA phantom	Air, PMMA, HA (50, 100, 200 mg cm^{-3}), aluminium	CT	Correlation CBCT-CT: All materials: $R^2 = 0.7014$–0.9996 Medium density: $R^2 = 0.5620$–0.9991 Error after calibration: 35–1562 GV
Plachtovics et al[61]	1	PMMA cylinder	PTFE, LDPE, acrylic, air, water	CT	Effect of phantom rotation: average shift, 15 GV (excluding air), maximum, 51 GV Effect of projection mode: average shift, 128 GV (excluding air), maximum, 263 GV Centre *vs* periphery (64 mm from centre): average shift, 209 GV; maximum, 240 GV (except double-exposure overlap mode: shift, 10 GV)
Reeves et al[62]	2	Reference object in patient's mouth	Cortical bone, trabecular bone, PMMA, water	Linear attenuation coefficients	Clinical application of Mah et al[48] <3% difference between average derived and actual Hounsfield units
Sennerby et al[63]	1	Cylindrical phantom with water bath	PE, PS, nylon, PC, PMMA, HA (200, 800, 1000, 1500 mg cm^{-3})	Linear attenuation coefficients, hydroxyapatite concentration	$R^2 = 0.9574$–0.9979 Effect of scan setting (binning): maximum shift, 10 GV Deviations up to 25 GV seen from correlation plots Variability up to approximately 20 GV between slices
Silva et al[64]	1	Mandibles ($n = 20$)	Trabecular bone	CT	Difference in average GV between CBCT and CT: 105 GV
Spin-Neto et al[65]	6	Human skull in acrylic	All voxels in FOV	N/A	GV shifts between consecutive exposures: <5 GV for four CBCTs, ≤17 GV and ≤109 GV for two other CBCTs

(Continued)

Table 1 (Continued)

Study	*CBCT models*	*Phantom*	*Materials*	*Reference*	*Results*[a]
Valiyaparambil et al[66]	1	Cylindrical phantoms ($n = 2$)	K_2HPO_4 (50–1000 mg ml^{-1}), HA (100, 200, 400, 800 mg cm^{-3})	CT	Correlation CBCT-CT: $R^2 = 0.98$–0.99
Yamashina et al[67]	1	Soft tissue-equivalent phantom in water container	Air, epoxy resin, water	CT	Reproducibility: average shift, 3 GV; maximum, 5 GV Effect of position in FOV: Air: maximum shift, 144 GV Epoxy resin: maximum shift, 107 GV Water: maximum shift, 129 GV

BMD, bone mineral density; CV, coefficient of variance; FOV, field of view; GV, gray value; HA, hydroxyapatite; K_2HPO_4, dipotassium phosphate; LDPE, low-density polyethylene; mgI, milligrams of iodine, N/A, not applicable; PC, polycarbonate; PE, polyethylene; PMMA, polymethyl methacrylate; POM, polyoxymethylene; PS, polystyrene; PTFE, polytetrafluoroethylene; PVC, polyvinyl chloride; SD, standard deviation.
[a]Recalculated to R^2 when explicitly stated that R was used. Certain results provided in this table were retrospectively derived from graphs and tables provided in the respective article.

Differences between CBCT models

Like snowflakes and fingerprints, no two CBCT models are the same, demonstrating essential differences in terms of exposure, hardware and reconstruction. This is a common limitation in all types of research performed on CBCT, as it is often limited to a single CBCT model for practical purposes. Therefore, findings on a certain CBCT model cannot be applied to any other model without experimental verification. Although it will not be mentioned further on, this is an important remark pertaining to most of the studies mentioned below. Out of 35 studies in Table 1, 23 (66%) include 1 CBCT model, and only 5 (14%) involve >3 models. Evidence found regarding stability or variability of GVs on one particular CBCT model cannot be considered as general truths that can be applied to CBCT as a whole, but certain trends or consistent findings can often be spotted.

Correlation is not enough

Correlation plots and coefficients, while extremely useful to display the dispersion of data to visualize trends and to identify outliers, have very limited value when interpreting data quantitatively. While a detailed mathematical and statistical elaboration is beyond the scope of this review, the limitations of correlation analysis will be illustrated with a few straightforward examples.

Initially, a distinction should be made between correlation coefficients (R) and coefficients of determination (R^2). The most commonly used correlation coefficient, the Pearson product–moment coefficient for paired samples, expresses linear correlation between variables, and ranges between −1 (perfect negative correlation) and +1 (perfect positive correlation) with a value of 0 implying no correlation. The coefficient of determination, however, describes the goodness of fit and ranges between zero (no fit) and one (perfect fit). R and R^2 are both used in literature but are not interchangeable, with R^2 being equal to the square of R for linear fits [when not forced to intercept at (0,0)]. In the literature overview below, values are provided as R^2 when possible (*i.e.* when explicitly mentioned by authors whether R or R^2 was used).

R and R^2 values in literature evaluating GV in CBCT are typically high, with values above 0.95 being common (Table 1). In addition, much lower R^2 values end up being statistically significant. Often, this is considered as proof that there is a potential for CBCT GV to be used as Hounsfield units. However, it can be demonstrated that large variability between actual and expected GV can occur even for high R-values. Figure 1 shows scatter plots of fictional data points resembling GV along a 12-bit scale, showing two types of deviations from a perfect linear relation: (1) deviation as a percentage of the value (*e.g.* ±20%) and (2) deviation as a fixed numerical value (*e.g.* 500 GV). R^2 values were calculated for various percentile and numerical deviations and are displayed in Table 2. It can be seen that, even for large deviations from a linear fit, R^2 values are high, and correlations are statistically significant. It is only at R^2 values close to 1 (>0.999) that these deviations are small enough to consider for clinical use (*e.g.* 1% or ±20 GV). Another issue related to R^2 is seen in Figure 2, which shows a ±20% deviation from a linear fit as in Figure 1, but with three of five data points clustered in the middle. Although deviations are still large, the clustering facilitates linear fitting and an increase in R^2 to 0.936 (from 0.924, without clustering) is seen. Two studies by Pauwels et al[59,60] take both of these issues into account, by calculating a separate R^2 for the medium density range or by calculating the error after Hounsfield unit calibration in addition to R^2.[59,60] In the former study, an overall decrease in R^2 was seen when excluding GVs for air and aluminium;[59] in the latter case,[60] considerable calibration errors where shown despite R^2 values being very high (>0.99). Other studies in which correlation is used often reveal large deviations in GV despite an R/R^2 value that was interpreted as high (Table 1).

Uniformity, a uniform issue

In several studies in Table 1, the applicability of Hounsfield units in CBCT is evaluated in "perfect"

conditions, with the evaluated region centred in the FOV. However, as mentioned above, uniformity of GVs in the axial plane is one of the main issues associated with the limited-FOV cone-beam geometry, and large differences between central and peripheral GVs may occur (Figure 3).

Various studies have evaluated this issue, with generally consistent findings. Pauwels et al[59] evaluated intra- and inter-scan uniformity in a homogeneous polymethyl methacrylate phantom as the relative difference in GV between central and peripheral regions of the image, finding difference of 3.3–21.1% with an average of 9.5% (*i.e.* approximately 100 GV on a Hounsfield unit scale) for seven CBCTs. Katsumata et al[44] noticed clear differences in GVs at the buccal and lingual sides of a mandible scanned in water. Lagravère et al[47] showed clear shifts in GV owing to the object's location (up to 85–214 GV, depending on the material), showing clear uniformity issues despite the fact that the statistical test came out as non-significant. Nackaerts et al[49] illustrated a lack of uniformity through the use of line profiles of a rectangular bone density phantom, demonstrating cupping/doming effects and calculating a 100-fold difference in variability of GV between CBCT and MDCT. They also showed a large effect of phantom orientation as well as central *vs* off-centre positioning. Molteni[28] showed a discrepancy between central and peripheral GV for water, ranging between −135 to + 125 GV. In addition, a difference of 114 GV was seen between an air pocket inside the phantom and air outside of it. Furthermore, phantom position (central or peripheral in the FOV) affected GVs. Plachtovics et al[61] found that a rotation of a centrally positioned, slightly asymmetrical phantom leads to GV shifts of 15 GV (maximum, 51 GV). In addition, they found mean GV differences between central and peripheral regions of 209 GV with a maximum of 240 GV. The use of a newly introduced double-exposure overlap reduced this shift to 10 GV, although a drop in GV was still noticeable at the edge of the image. Bujtár et al[38] showed that varying positions of reference objects placed in a cadaver head leads to standard deviations of GV between 70 and 135 with maximum shifts of 193–488, depending on the reference material.

Effect of endo- and exo-mass on gray value

Several studies have shown shifts in GVs owing to the amount of mass inside the FOV as well as an effect of objects outside it. Bryant et al[37] showed the effect of the total mass in a slice and of the presence of an asymmetrical mass outside the FOV, although the central (approximately 70%) of the (large-diameter) FOV showed stable GVs for the evaluated CBCT model. Molteni[28] showed the effect of exo-mass and the presence of water. Mah et al[48] used a small cylindrical phantom scanned in air and in a small/large water container, showing an average GV shift of 127 with a maximum of 1258 owing to the change in total mass of the scanned object. Nomura et al[54] showed large differences of GVs when using water and air as background materials, with GV-density regression lines also sloped differently.

Pauwels et al[60] showed a poor GV–Hounsfield unit correlation for certain small-FOV CBCTs when scanning each material separately. This was due to histogram shifting, which is a reconstruction technique that optimizes image contrast by assigning GVs depending on the amount and distribution of densities inside the FOV. For example, the presence of a high-density object will shift GVs towards the left of the histogram (*i.e.* lower GVs).

The presence of an asymmetrical mass outside the FOV can affect the numerical GV as well as inducing a shading effect. Katsumata et al[44] showed that the presence of objects outside the FOV can shift GVs up to 10%; even after GVs were normalized to those of bone to obtain a relative density estimation. Nomura et al[54] showed a slighter shift of GV owing to the presence of hard tissue (6 GV; maximum, 9 GV) and metal inside (15 GV; maximum, 30 GV) and outside (13 GV; maximum, 28 GV) the FOV. While Oliveira et al[55] found a large shift (average, 183 GV) owing to the presence of an exo-mass, the addition of an implant inside the FOV showed a marginal effect (average, 5 GV) for all but one (28 GV) exposure protocol.

Differences in GV owing to FOV size, apart from possible differences in scatter and reconstruction, can be attributed to the variable amount of endo- and exo-mass for small- and large-diameter FOVs. Katsumata et al[45] showed inconsistent GVs between different FOVs, with differences up to 374 GV. They showed reduced GV variability for larger FOVs. Molteni,[28] on the other hand, noticed reduced artefacts for smaller FOVs. Parsa et al[58] showed differences up to 402 GV/116 GV for two CBCT models owing to the use of different available FOV sizes.

Variability between slices

The variability of GVs between axial slices (*i.e.* between the top, middle and bottom parts of the FOV) cannot be fully attributed to varying amounts of endo-mass, as deviations have been shown even for homogeneous objects. However, studies investigating the cause and severity of GV variability along the *z*-axis are scarce. Sennerby et al[63] shows a maximum difference of approximately 20 GV between axial slices, while Molteni[28] showed an increase in GVs towards the top of the FOV for one CBCT model, showing differences of approximately 50 GV for air. Nomura et al[54] demonstrated overall constant, yet spiky, line profiles of GVs along the *z*-axis, with standard deviations of 8.3–10.8 GV. Bamba et al,[36] in a study involving three CBCT models and various imaging parameters and set-ups, showed stable GVs in the coronal plane for certain scans but moderate variation along the *z*-axis in some cases. Hohlweg-Majert et al[43] demonstrated average shifts of 24 GV (maximum, 67 GV) between axial slices in CBCT. Nishino et al[52] varied the position of a cylindrical phantom along the *z*-axis, showing shifts up to 19–69 GV, depending on the material. Figure 4 shows stable GVs

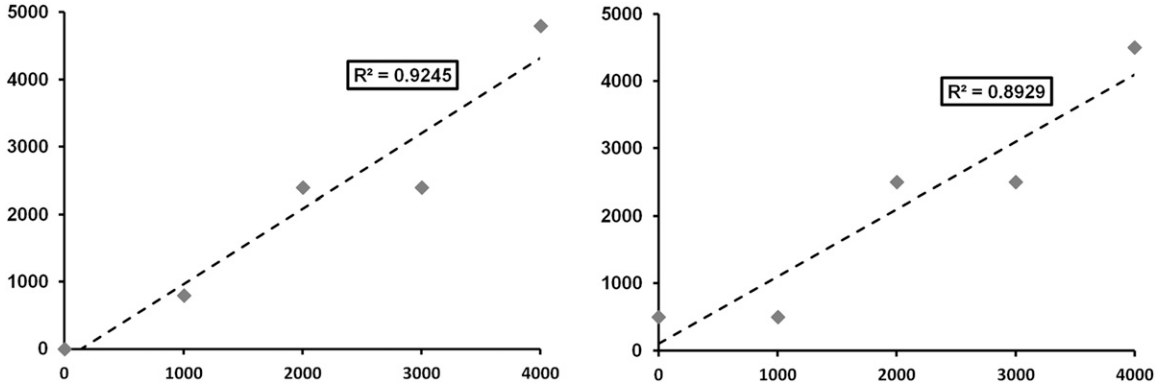

Figure 1 Scatter plots for values showing a deviation of ±20% (left) and ±500 GV (right). R^2 values are high despite the large deviations. The data points used for these graphs were determined for the purpose of illustration, that is, they are not the result of experimentation.

along the *z*-axis for different FOV heights for one CBCT model for a water phantom, with maximum differences of 5–9 GV and standard deviation values of 0.6–1.4 GV. It can be noticed that numerical GVs can differ considerably between FOVs, which is likely due to histogram shifting. Further evidence on other CBCT models is required before variability of GVs along the *z*-axis can be considered as an effect inherent to the CBCT exposure geometry.

Variability owing to changing exposure parameters

Potential differences in GVs owing to FOV size has been described in the above subsection on the effect of endo- and exo-mass. While variations in beam energy are expected to lead to a change in GV (as attenuation coefficients depend on X-ray energy), variations in mA and exposure time should not affect numerical GVs. On the other hand, an increase in mAs may lead to a marginal improvement in GV variability, especially when measuring in small regions, owing to a decrease in noise. Little information is available on this, with Pauwels et al[60] showing no improvement in CBCT–MDCT correlation for high-dose CBCT protocols. Sennerby et al[63] showed differences up to 10 GV owing to detector binning. Molteni[28] found no difference for high- and low-resolution modes. Plachtovics et al[61] measured average GV shifts of 128 GV (maximum, 263 GV) owing to the use of different exposure modes. Nomura et al[53] noticed slight differences, mostly <10 GV, owing to varying kVp/mA settings. A more pronounced effect was found by Oliveira et al,[55] showing an average shift of 122 GV owing to varying kVp and 40 GV owing to varying mA settings. Parsa et al[58] showed small (3 GV)-to-moderate (36 GV) effects of varying mA and exposure time (resolution mode or 360° *vs* 180° rotation) for two CBCT models. Bamba et al[36] investigated various combinations of kVp, mA and exposure time for three CBCT models, showing considerable effects on GV distributions. An interesting finding by Spin-Neto et al[65] was that, even when exposure parameters are kept constant, the amount of and time between consecutive exposures (*i.e.* the workload of CBCT) can have some effect on the GV distribution.

Table 2 R^2 values for plots of five *x*, *y* data points, where *y* deviates from *x* as a percentage or a fixed amount of gray values (GVs)

Deviation	R^2
±20%[a]	0.9245
±10%	0.9777
±5%	0.9940
±1%	0.9997
±500 GV[a]	0.8929
±250 GV	0.9709
±100 GV	0.9952
±20 GV	0.9998

All R^2 values are statistically significant ($p < 0.01$). The data points used for these tables were determined for the purpose of illustration, that is, they are not the result of experimentation.
[a]Illustrated in Figure 1.

Hounsfield units calibration/correction

In several studies, an attempt was made to calibrate GVs along a Hounsfield unit or density scale or to correct for discrepancies caused by a lack of uniformity or endo- and exo-mass. While results often seem promising, a

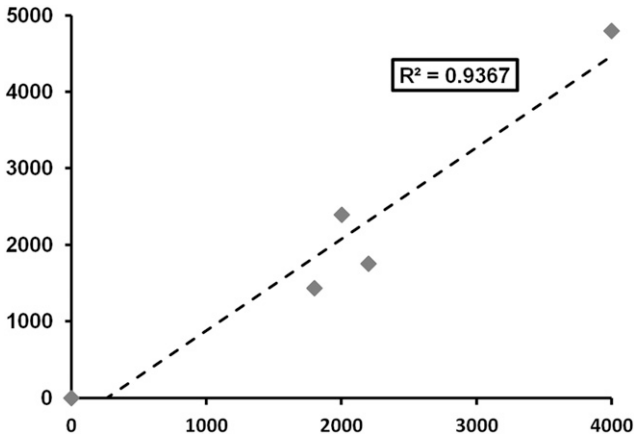

Figure 2 Increased R^2 value owing to clustering of data points. Deviations (as a percentage) are identical to those in Figure 1 (left). The data points used for this graph were determined for the purpose of illustration, that is, they are not the result of experimentation.

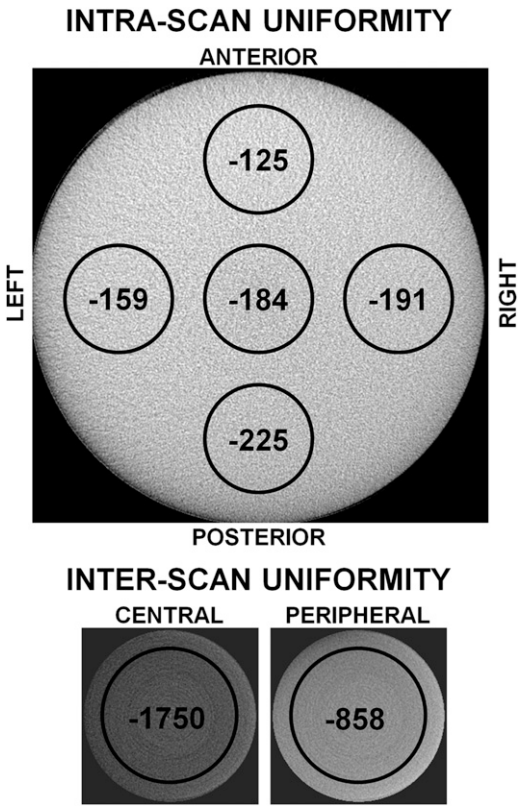

Figure 3 Uniformity issues in CBCT, measured using a 160-mm homogeneous polymethyl methacrylate phantom. Each black circle shows the mean gray value inside it. Top: intrascan uniformity, showing differences in gray values between central and peripheral regions for a large-diameter (160 mm) CBCT scan. Bottom: interscan uniformity, showing differences between central and peripheral field of view positions for a small-diameter (50 mm) CBCT scan. The bottom two images are displayed using the same window/level settings. All images are to scale.

common limitation is that these approaches were validated using the very data that they were derived from, and are likely not applicable for other CBCT models or varying exposure conditions.

As mentioned above, Pauwels et al used CT-derived GVs for air and aluminium as calibration points to estimate GVs for polymethyl methacrylate and hydroxyapatite for 13 CBCT models. However, this was carried out for the purpose of error estimation rather than Hounsfield unit calibration, and it was seen that errors can still be considerable after calibration, with a minimum error of 35 GV and an average error of 110 GV for protocols with a very high correlation ($R > 0.99$), and much higher error values for protocols with a lower correlation.[60]

Mah et al[48] derived Hounsfield units using attenuation coefficients at an effective beam energy. Although a high correlation was seen, large differences in derived Hounsfield units between CBCTs were shown, even for similar beam energies. Reeves et al[62] applied the findings of Mah et al in a clinical setting, showing a <3% difference between derived and actual Hounsfield units using a reference object placed in the patient's mouth. Although the use of intrascan reference objects is most likely the best approach to use CBCT GVs in a quantitative way, variability of GVs in the axial plane and along the *z*-axis are not taken into account using this method. In addition, reference materials placed in a bite block can be severely affected by metal artefacts from dental restorations.

Naitoh et al[50] used a sample of patients who underwent CBCT and MDCT scanning to define regression lines estimating BMD from CBCT GVs. Correlation results were considered as "high", but scatter plots showed deviations of up to approximately 200 GV from the fitted line. In a second study, Naitoh et al used a reference block to estimate BMD from CBCT, which deviated 1–123 mg cm^{-3} (average, 38 mg cm^{-3}) from values derived from MDCT. 84% of bone sites were correctly classified as being above or below 200 mg cm^{-3} using the reference block, although less than half of patients were in the 150–250 mg cm^{-3} range, approximately 38% of which were misclassified. All but one of the misclassifications were overestimations of BMD, indicating that an adjustment of the regression line may be warranted.[51]

Bryant et al[37] proposed a correction equation, noticing that the investigated CBCT scanner showed correct Hounsfield units when the mass in a slice was 5 g, while the mass in an adult head was estimated at 7 g for a slice thickness of 0.4 mm. This correction should be verified on other CBCT scanners; also, the effect of varying mass per slice should be taken into account, as the correction assumes a uniform density of 1.05 g cm^{-3}. In addition, Bryant et al[37] proposed a correction for the GV gradient owing to the exo-mass effect. While this second correction noticeably improved GV balance, differences of 300 GV units remained between the anterior and posterior side of the scan. This correction method should be validated for different degrees of exo-mass and other CBCT scanners.

Lagravère et al[46] determined a regression equation to directly estimate density based on CBCT GVs, showing a standard error of 27 GV. In a second study by Lagravère

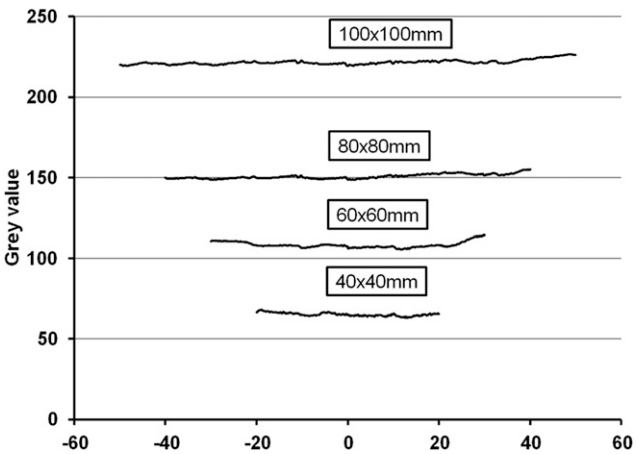

Figure 4 Variability of gray values (GVs) along the *z*-axis for four fields of view (FOVs) of the 3D Accuitomo 170 (J. Morita, Kyoto, Japan) for a water phantom. GVs for the 100 × 100-mm FOV were reduced by 100 for plotting purposes.

et al,[47] using a more recent CBCT model from the same manufacturer, a considerably different regression equation was found. Correlations found in both studies (R^2, 0.893–0.986) can be considered as low, based on the considerations in the above subsection.

Plachtovics et al[61] proposed a double-exposure overlap acquisition, consisting two consecutive (or simultaneous) full-rotation exposures with a relatively low number of projections. Compared with single-rotation protocols, the double-exposure protocol showed a notable improvement in GV uniformity throughout the axial plane (except at the very edge of the FOV) as well as a more accurate Hounsfield unit calibration. The potential benefit of this type of exposure in terms of overall image quality and GV accuracy warrants further investigation.

Literature review: clinical application of gray value in CBCT

Several studies have investigated the potential clinical application of CBCT GVs in clinical or simulated situations. Several applications have been considered, ranging from bone density assessment to differential diagnosis of lesions (Table 3).

CBCT GVs have been compared with several clinical bone parameters by various authors. Sennerby et al[63] assessed bone density for implant placement on 49 patients. A low correlation was found between GV, resonance frequency and insertion torque ($R^2 = 0.21$–0.31), although there may be an actual lack of correlation between these parameters on top of a variability of GVs obtained from CBCT. Fuster-Torres et al[70] did a similar analysis, also finding a relatively low correlation between GV, resonance frequency and insertion torque ($R^2 =$ 0.00–0.55). Lee et al[72] found similar Spearman correlation coefficients (R) for CBCT and MDCT GVs compared with subjective drilling resistance ($R = 0.59$–0.61) and implant insertion torque ($R = 0.61$–0.63). Song et al[74] found correlation coefficients of 0.29–0.75 between CBCT GV and implant stability quotients. Tatli et al[75] reported a Spearman correlation (R) of 0.54–0.87 between CBCT GV and implant stability quotients at four time points, as well as a negative correlation ($R = -0.47$) between GVs and stability loss. Aranyarachkul et al[34] found a Spearman correlation (R) of 0.46–0.60 comparing CBCT GVs with Lekholm–Zarb ratings. Brosh et al[69] assessed bone quality at inter-radicular sites for the purpose of mini-implant placement on eight swine bones. Considering all sites for each jaw, a correlation (R^2) of 0.70 (maxilla) to 0.75 (mandible) was seen between GV and hardness. Also, looking at individual sites, no correlation was found for maxillary sites and one out of four mandibular sites. Considering all of the above studies and depending on the expected predictive value and the definition of new bone classification methods, interpatient variability associated with these correlation results are likely too large to consider clinical application of CBCT GV as a reliable predictor of bone quality for implant placement.

Barone et al[68] evaluated the effect of immediate implant loading using CBCT, finding higher GV compared with delayed loading on a small patient sample (6 patients, 12 implants). GVs were used in a relative way, scaling between 0 (water) and 100 (titanium). Validation of this type of approach using varying exposure conditions is warranted before clinical use is considered. It should also be noted that the routine use of CBCT after implant placement should be avoided owing to radioprotection concerns.[76–78]

Kaya et al[71] investigated bony changes in periapical lesions before and 2 years after treatment on 16 patients. They found a significant increase in GVs after treatment, using GVs in a relative way rather than trying to calculate actual bone density. Pre- and post-treatment comparison of CBCT GV can be feasible when scanning patients under the same exposure conditions. To validate the use of CBCT for this purpose, further investigations on more subtle bone changes is warranted, seeing that the changes in this study were too obvious, with increases in GVs averaging at +363 GV.[71] Furthermore, routine use of CBCT after endodontic treatment is ill-advised in the absence of complications or symptoms owing to the increased radiation dose compared with two-dimensional radiography.[78–81]

Simon et al[73] applied GV for the differential diagnosis of periapical lesions, using a threshold (TH) of GV = 0 to distinguish between cysts and granulomas. For 13/17 cases, agreement was seen between CBCT finding and biopsy. In all four other cases, biopsy revealed granulomas, whereas CBCT GVs pointed to cysts. Considering the detection of granulomas, the sensitivity of this study was 60%, which does not seem adequate despite the specificity being 100%. However, the authors themselves questioned the validity of the biopsy findings, which complicates the interpretation of the results. Although more investigation on this topic is warranted, it is important to note that this classification method is highly dependent on the accuracy of the 0-value (*i.e.* the GV for water), which should be verified through phantoms and, if needed, corrected before considering clinical application.

Alternative methods for bone evaluation

From density to quality

The lack of GV standardization is a major problem for most CBCT devices, yet considering the fact that a healthy vascularized bone structure may be more clinically relevant, the Hounsfield unit limits for implant treatment may be easily overcome. Following the aforementioned statements on the need for healthy vascularized and well-structured trabecular bone, the clinical use of regional trabecular density by analysis of Hounsfield units and/or BMD should be questioned, even when associations with the Lekholm and Zarb[24] index as well as with implant treatment outcome have been previously established. Yet, apart from the fact that the qualitative scoring methods and the density assessment have become

Table 3 Studies applying gray value (GV) CBCT quantitatively

Study	*CBCT models*	*Patients*	*Application*	*Results*[a]
Aranyarachkul et al[34]	1	9 human cadavers (63 sites)	Bone density for implant placement	Spearman correlation (R) with Lekholm–Zalb ratings, 0.46–0.60
Barone et al[68]	1	6 (12 sites)	Bone density after implant placement	Higher relative GVs for immediate implant loading, +5.2% (para-axial), +6.8% (axial)
Brosh et al[69]	1	8 swine bones	Bone quality at inter-radicular sites for mini-implant placement	Correlation between GV and hardness: 0.70 (maxilla)–0.75 (mandible). Correlation for individual sites only found in mandible.
Fuster-Torres et al[70]	1	22	Bone density for implant placement	Correlation between GV, resonance frequency and insertion torque, $R^2 = 0.000$–0.548 (average, 0.071)
Kaya et al[71]	1	16	Bone density in periapical lesions, pre- and post-treatment (2 years)	Significant differences between GV pre- and post-treatment
Lee et al[72]	1	42 human cadavers	Bone density (osteotomy and implant placement)	Similar Spearman correlation (R) for CBCT and multidetector CT GVs *vs* subjective drilling resistance (0.59–0.61) and implant insertion resistance torque (0.61–0.63).
Sennerby et al[63]	1	49	Bone density for implant placement, pre and post (6 month)	Correlation between GV, resonance frequency and insertion torque, $R^2 = 0.21$–0.31
Simon et al[73]	1	17	Differential diagnosis of periapical lesions	13/17 cases showed correspondence between CBCT GV and biopsy Validity of biopsy questioned for four other cases
Song et al[74]	1	20	Bone density for implant placement	Correlation coefficient for CBCT GVs and implant stability quotients, 0.2887–0.7525
Tatli et al[75]	1	23 (77 implants)	Bone density for implant placement	Spearman correlation of CBCT GVs *vs* implant stability quotients at four time points, $R = 0.544$–0.874 CBCT GV *vs* stability loss, $R = -0.470$

[a]Recalculated to R^2 when explicitly stated that R was used.

seemingly less interesting, it is also well established that scoring systems like the widespread Lekholm–Zarb index are prone to bias. Results from such scorings are highly variable and subjective, while correlation with bone density show a wide variation.[5,13,14,22,23] Furthermore, only a weak correlation between the mechanical properties of fresh mandibular bone and Hounsfield units/BMD may exist,[82] insufficient to accurately predict the mechanical bone properties. The latter is confirmed in more recent orthopaedic studies claiming that current implant systems for hip replacement do not necessarily require high-density bone.[83] As mentioned above, what is currently needed for successful osseointegration is a healthy and well-vascularized bone.

Bone structure analysis

Owing to the various limitations related to the quantitative use of GVs in CBCT as well as the recent evolution in implant dentistry to go beyond the evaluation of bone density, and thanks to the increasingly improving image quality in CBCT owing to innovations in hardware and software, alternative methods for analysing bone structure have recently gained attention. Several studies have reported on the potential application of bone structure parameters commonly used in microscopy and μCT. Although evidence regarding accuracy and stability of these parameters is still limited, certain parameters have shown potential for clinical applications. de Oliveira et al[11] identified four characteristics of bone tissue microarchitecture by μCT at dental implant bone sites, which might be applicable for clinical bone quality evaluation, including (1) 3D trabecular bone architecture, (2) bone surface (BS)/volume ratios expressing bone density, (3) bulk or amount of bone and (4) spacing between trabeculae and marrow spaces. This structural analysis has clinical potential for pre-surgical assessment of bone. In this section, a brief overview will be provided of parameters with potential clinical application.

To estimate the amount and dispersion of bone within a bony region, bone volume (BV) and BS are used, often normalized to the total volume of the region of interest. These parameters are complimentary, for example, a homogenous piece of bone will have a high BV but low BS value since only the exterior surface contributes to the BS, whereas a network of trabecular bone will have a relatively higher BS value for a given BV. BV and BS are easily interpretable and are among the most feasible alternative bone parameters to measure on CBCT images. Still, when compared with high-resolution

gold standards such as μCT and histology, CBCT images are much more blurry, leading to a consistent overestimation of BV due to partial volume averaging and an underestimation of BS due to a loss of fine structures. In addition, the clinical relevance of BV and BS is limited, as they do not reflect the true bone structure. A more abstract bone metric is fractal dimension, which is measured using the box-counting method.[84] Simply put, this method scans an image using boxes of decreasing sizes, and counts the proportion of boxes containing bone. While various studies applied fractal dimension on *in vitro*, animal and clinical CBCT data,[85–88] its stability and clinical value should be further explored.

Various structural bone parameters exist, and their applicability and clinical relevance for CBCT imaging has recently gained attention. A selection of parameters will be briefly discussed here. Firstly, a bone image can be skeletonized, which is a form of erosion resulting in structures being iteratively thinned until their centre lines remain.[89] The remaining skeleton branches and junctions can then be analysed. Although this is an interesting and easily interpretable analysis, it is highly dependent on the proper visualization of individual trabeculae, and its values are grossly underestimated on CBCT images compared with μCT. Another type of structural analysis is connectivity, which estimates the number of connected structures in a network.[90] It can be interpreted in a similar way as skeleton analysis, but, likewise, its value depends on the visualization of individual trabeculae, requiring a very high image sharpness. Another parameter that requires the depiction of individual trabeculae is thickness/spacing, which, as its name implies, represents the thickness of trabeculae and the spacing between them.[91]

Different structural parameters, most notably structure model index and plateness have been designed to express the extent of rod- or plate-like geometry in bone.[92] Similar to fractal dimension, further evidence on the stability and clinical relevance of these parameters is needed. The same statement applies to other bone parameters not covered in this article.

A limitation applying to all bone parameters mentioned in this section is that they are measured on thresholded, binary (*i.e.* black and white) images. This implies that before analysis, a TH between GVs for the bone and other tissues needs to be determined. Results will vary considerably depending on the TH value, because the selection of an inappropriate TH could lead to severe under- or overestimations of the amount of bone and may lead to a loss of bone structure on the binary image. It should be clear from the section above that a fixed TH value is not currently applicable on CBCT images owing to the lack of consistent GVs. Although a plethora of TH algorithms are available that are independent of the numerical GV, a standardized thresholding method for trabecular and/or cortical bone on dental CBCT images is yet to be determined.

Although several authors have found a correlation between bone quantity and bone structure parameters on CBCT and μCT or dual-energy X-ray absorptiometry images (Figure 5),[57,85,93–95] the limitations to the use of correlation analysis mentioned above apply here as well. To consider these parameters for clinical use, a very high correlation would need to be demonstrated, as well as stable inter- and intra-CBCT values (*i.e.* independent from exposure parameters, type of equipment etc.).[96,97] Further validation of the clinical relevance, stability and reproducibility of these parameters on CBCT images is warranted, which would require a combination of *in vitro* studies with retrospective or prospective evaluations of patient outcome. If certain parameters can be validated and a consistent relation is found with clinical bone quality, classification schemes based on these parameters, similar to existing bone classifications, could be devised.

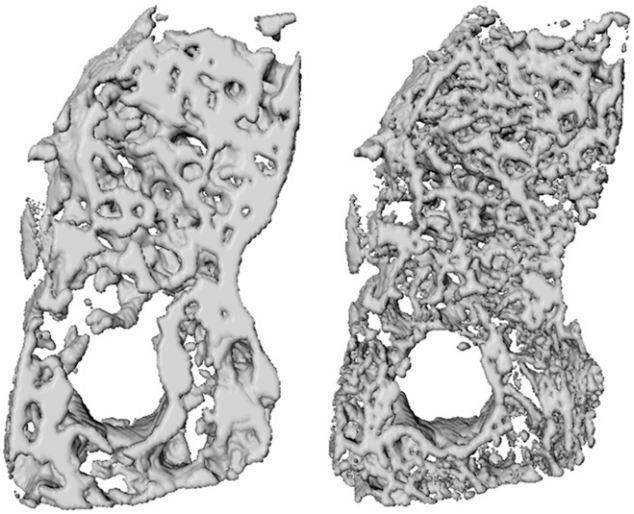

Figure 5 Volume renderings of a mandibular bone sample scanned with CBCT (left) and micro-CT (right). Despite the difference in spatial resolution, similarities in bone structure visualization can be observed. Adapted from Van Dessel et al.[93]

Conclusion

Although there can be a limited use of quantitative GVs in CBCT in some cases, it should be generally avoided owing to its unreliability. GVs, measured on CBCT images may shift owing to the use of different CBCT devices, exposure parameters, the position of the measurement in the FOV (centrally *vs* peripherally) and the amount of mass inside and outside the FOV.

Developments in CBCT imaging as well as the use of advanced GV correction techniques may increase the potential of applying CBCT-derived GVs, such as CT-derived Hounsfield units, but the main focus in research should be on the clinical validation of alternative parameters for the evaluation of bone structure, as they may be more suited to predict implant outcome than bone density alone.

References

1. Lambert FE, Weber HP, Susarla SM, Belser UC, Gallucci GO. Descriptive analysis of implant and prosthodontic survival rates with fixed implant-supported rehabilitations in the edentulous maxilla. *J Periodontol* 2009; **80**: 1220–30. doi: 10.1902/jop.2009.090109
2. Vercruyssen M, Marcelis K, Coucke W, Naert I, Quirynen M. Long-term, retrospective evaluation (implant and patient-centred outcome) of the two-implants-supported overdenture in the mandible. Part 1: survival rate. *Clin Oral Implants Res* 2010; **21**: 357–65. doi: 10.1111/j.1600-0501.2009.01849.x
3. Chen H, Liu N, Xu X, Qu X, Lu E. Smoking, radiotherapy, diabetes and osteoporosis as risk factors for dental implant failure: a meta-analysis. *PLoS One* 2013; **8**: e71955. doi: 10.1371/journal.pone.0071955
4. Jacobs R. Preoperative radiologic planning of implant surgery in compromised patients. *Periodontol 2000* 2003; **33**: 12–25.
5. Merheb J, Van Assche N, Coucke W, Jacobs R, Naert I, Quirynen M. Relationship between cortical bone thickness or computerized tomography-derived bone density values and implant stability. *Clin Oral Implants Res* 2010; **21**: 612–17. doi: 10.1111/j.1600-0501.2009.01880.x
6. Bass SL, Triplett RG. The effects of preoperative resorption and jaw anatomy on implant success. A report of 303 cases. *Clin Oral Implants Res* 1991; **2**: 193–8.
7. de Oliveira RC, Leles CR, Lindh C, Ribeiro-Rotta RF. Bone tissue microarchitectural characteristics at dental implant sites. Part 1: identification of clinical-related parameters. *Clin Oral Implants Res* 2012; **23**: 981–6. doi: 10.1111/j.1600-0501.2011.02243.x
8. Jemt T, Lekholm U. Implant treatment in edentulous maxilla: a five year follow-up report on patients with different degrees of jaw resorption. *Int J Oral Maxillofac Implants* 1995; **10**: 303–11.
9. Quirynen M, Gijbels F, Jacobs R. An infected jawbone site compromising successful osseointegration. *Periodontol 2000* 2003; **33**: 129–44.
10. Marx RE. A decade of bisphosphonate bone complications: what it has taught us about bone physiology. *Int J Oral Maxillofac Implants* 2014; **29**: e247–58. doi: 10.11607/jomi.te61
11. de Oliveira MA, Asahi DA, Silveira CA, Lima LA, Glick M, Gallottini M. The effects of zoledronic acid and dexamethasone on osseointegration of endosseous implants: histological and histomorphometrical evaluation in rats. *Clin Oral Implants Res* Jan 2014. Epub ahead of print. doi: 10.1111/clr.12335
12. Zuffetti F, Testori T, Capelli M, Rossi MC, Del Fabbro M. The topical administration of bisphosphonates in implant surgery: a randomized split-mouth prospective study with a follow-up up to 5 Years. *Clin Implant Dent Relat Res* Sep 2013. Epub ahead of print. doi: 10.1111/cid.12151
13. Merheb J, Coucke W, Jacobs R, Naert I, Quirynen M. Influence of bony defects on implant stability. *Clin Oral Implants Res* 2010; **21**: 919–23. doi: 10.1111/j.1600-0501.2010.01932.x
14. Ribeiro-Rotta RF, Lindh C, Pereira AC, Rohlin M. Ambiguity in bone tissue characteristics as presented in studies on dental implant planning and placement: a systematic review. *Clin Oral Implants Res* 2011; **22**: 789–801. doi: 10.1111/j.1600-0501.2010.02041.x
15. Ribeiro-Rotta RF, Pereira AC, Oliveira GH, Freire MC, Leles CR, Lindh C. An exploratory survey of diagnostic methods for bone quality assessment used by Brazilian dental implant specialists. *J Oral Rehabil* 2010; **37**: 698–703. doi: 10.1111/j.1365-2842.2010.02102.x
16. Engquist B, Bergendal T, Kallus T, Linden U. A retrospective multicenter evaluation of osseointegrated implants supporting overdentures. *Int J Oral Maxillofac Implants* 1988; **3**: 129–34.
17. Jemt T, Book K, Lindén B, Urde G. Failures and complications in 92 consecutively inserted overdentures supported by Brånemark implants in severely resorbed edentulous maxillae: a study from prosthetic treatment to first annual check-up. *Int J Oral Maxillofac Implants* 1992; **7**: 162–7.
18. Jaffin RA, Berman CL. The excessive loss of Branemark fixtures in type IV bone: a 5-year analysis. *J Periodontol* 1991; **62**: 2–4.
19. Lindh C, Petersson A, Rohlin M. Assessment of the trabecular pattern before endosseous implant treatment: diagnostic outcome of periapical radiography in the mandible. *Oral Surg Oral Med Oral Pathol Oral Radiol Endod* 1996; **82**: 335–43.
20. Benson BW, Prihoda TJ, Glass BJ. Variations in adult cortical bone mass as measured by a panoramic mandibular index. *Oral Surg Oral Med Oral Pathol* 1991; **71**: 349–56.
21. Klemetti E, Kolmakov S, Heiskanen P, Vainio P, Lassila V. Panoramic mandibular index and bone mineral densities in postmenopausal women. *Oral Surg Oral Med Oral Pathol* 1993; **75**: 774–9.
22. Norton MR, Gamble C. Bone classification: an objective scale of bone density using the computerized tomography scan. *Clin Oral Implants Res* 2001; **12**: 79–84.
23. Misch CE. Density of bone: effect on treatment plans, surgical approach, healing, and progressive boen loading. *Int J Oral Implantol* 1990; **6**: 23–31.
24. Lekholm U, Zarb GA. Patient selection and preparation. In: Branemark P-I, Zarb GA, Albrektsson T, eds. *Tissue integrated prosthesis; osseointegration in clinical dentistry*. Chicago: Quintessence; 1985. pp. 199–209.
25. Alsaadi G, Quirynen M, Michiels K, Teughels W, Komárek A, van Steenberghe D. Impact of local and systemic factors on the incidence of failures up to abutment connection with modified surface oral implants. *J Clin Periodontol* 2008; **35**: 51–7.
26. Schulze R, Heil U, Gross D, Bruellmann DD, Dranischnikow E, Schwanecke U, et al. Artefacts in CBCT: a review. *Dentomaxillofac Radiol* 2011; **40**: 265–73. doi: 10.1259/dmfr/30642039
27. Pauwels R, Araki K, Siewerdsen JH, Thongvigitmanee SS. Technical aspects of dental cone-beam CT: state of the art. *Dentomaxillofac Radiol* 2014; **44**: 20140224. doi: 10.1259/dmfr.20140224
28. Molteni R. Prospects and challenges of rendering tissue density in Hounsfield units for cone beam computed tomography. *Oral Surg Oral Med Oral Pathol Oral Radiol* 2013; **116**: 105–19. doi: 10.1016/j.oooo.2013.04.013
29. Mullen A, Kron T, Thomas J, Foroudi F. Variations in cone beam CT numbers as a function of patient size: *in vivo* demonstration in bladder cancer patients. *J Med Imaging Radiat Oncol* 2010; **54**: 505–7. doi: 10.1111/j.1754-9485.2010.02203.x
30. Srinivasan K, Mohammadi M, Shepherd J. Cone beam computed tomography (CBCT) for adaptive radiotherapy treatment planning. *J Med Biol Eng* 2014; **34**: 377–85.
31. Hatton J, McCurdy B, Greer PB. Cone beam computerized tomography: the effect of calibration of the Hounsfield unit number to electron density on dose calculation accuracy for adaptive radiation therapy. *Phys Med Biol* 2009; **54**: N329–46. doi: 10.1088/0031-9155/54/15/N01
32. Li J, Yao W, Xiao Y, Yu Y. Feasibility of improving cone-beam CT number consistency using a scatter correction algorithm. *J Appl Clin Med Phys* 2013; **14**: 4346. doi: 10.1120/jacmp.v14i6.4346
33. Liu Y, Bäuerle T, Pan L, Dimitrakopoulou-Strauss A, Strauss LG, Heiss C, et al. Calibration of cone beam CT using relative attenuation ratio for quantitative assessment of bone density: a small animal study. *Int J Comput Assist Radiol Surg* 2013; **8**: 733–9. doi: 10.1007/s11548-012-0803-5
34. Aranyarachkul P, Caruso J, Gantes B, Schulz E, Riggs M, Dus I, et al. Bone density assessments of dental implant sites: 2. Quantitative cone-beam computerized tomography. *Int J Oral Maxillofac Implants* 2005; **20**: 416–24.
35. Azeredo F, de Menezes LM, Enciso R, Weissheimer A, de Oliveira RB. Computed gray levels in multislice and cone-beam computed tomography. *Am J Orthod Dentofacial Orthop* 2013; **144**: 147–55. doi: 10.1016/j.ajodo.2013.03.013
36. Bamba J, Araki K, Endo A, Okano T. Image quality assessment of three cone beam CT machines using the SEDENTEXCT CT phantom. *Dentomaxillofac Radiol* 2013; **42**: 20120445. doi: 10.1259/dmfr.20120445
37. Bryant JA, Drage NA, Richmond S. Study of the scan uniformity from an i-CAT cone beam computed tomography dental imaging

system. *Dentomaxillofac Radiol* 2008; **37**: 365–74. doi: 10.1259/dmfr/13227258
38. Bujtár P, Simonovics J, Zombori G, Fejer Z, Szucs A, Bojtos A, et al. Internal or in-scan validation: a method to assess CBCT and MSCT gray scales using a human cadaver. *Oral Surg Oral Med Oral Pathol Oral Radiol* 2014; **117**: 768–79. doi: 10.1016/j.oooo.2014.02.012
39. Cassetta M, Stefanelli LV, Di Carlo S, Pompa G, Barbato E. The accuracy of CBCT in measuring jaws bone density. *Eur Rev Med Pharmacol Sci* 2012; **16**: 1425–9.
40. Cassetta M, Stefanelli LV, Pacifici A, Pacifici L, Barbato E. How accurate is CBCT in measuring bone density? a comparative CBCT-CT *in vitro* study. *Clin Implant Dent Relat Res* 2014; **16**: 471–8. doi: 10.1111/cid.12027
41. Chindasombatjaroen J, Kakimoto N, Shimamoto H, Murakami S, Furukawa S. Correlation between pixel values in a cone-beam computed tomographic scanner and the computed tomographic values in a multidetector row computed tomographic scanner. *J Comput Assist Tomogr* 2011; **35**: 662–5. doi: 10.1097/RCT.0b013e31822d9725
42. Eskandarloo A, Abdinian M, Salemi F, Hashemzadeh Z, Safaei M. Effect of object location on the density measurement in cone-beam computed tomography versus multislice computed tomography. *Dent Res J (Isfahan)* 2012; **9**: S81–7.
43. Hohlweg-Majert B, Metzger MC, Kummer T, Schulze D. Morphometric analysis—cone beam computed tomography to predict bone quality and quantity. *J Craniomaxillofac Surg* 2011; **39**: 330–4. doi: 10.1016/j.jcms.2010.10.002
44. Katsumata A, Hirukawa A, Okumura S, Naitoh M, Fujishita M, Ariji E, et al. Effects of image artifacts on gray-value density in limited-volume cone-beam computerized tomography. *Oral Surg Oral Med Oral Pathol Oral Radiol Endod* 2007; **104**: 829–36.
45. Katsumata A, Hirukawa A, Okumura S, Naitoh M, Fujishita M, Ariji E, et al. Relationship between density variability and imaging volume size in cone-beam computerized tomographic scanning of the maxillofacial region: an *in vitro* study. *Oral Surg Oral Med Oral Pathol Oral Radiol Endod* 2009; **107**: 420–5. doi: 10.1016/j.tripleo.2008.05.049
46. Lagravère MO, Fang Y, Carey J, Toogood RW, Packota GV, Major PW. Density conversion factor determined using a cone-beam computed tomography unit NewTom QR-DVT 9000. *Dentomaxillofac Radiol* 2006; **35**: 407–9.
47. Lagravère MO, Carey J, Ben-Zvi M, Packota GV, Major PW. Effect of object location on the density measurement and Hounsfield conversion in a NewTom 3G cone beam computed tomography unit. *Dentomaxillofac Radiol* 2008; **37**: 305–8. doi: 10.1259/dmfr/65993482
48. Mah P, Reeves TE, McDavid WD. Deriving Hounsfield units using grey levels in cone beam computed tomography. *Dentomaxillofac Radiol* 2010; **39**: 323–35. doi: 10.1259/dmfr/19603304
49. Nackaerts O, Maes F, Yan H, Couto Souza P, Pauwels R, Jacobs R. Analysis of intensity variability in multislice and cone beam computed tomography. *Clin Oral Implants Res* 2011; **22**: 873–9. doi: 10.1111/j.1600-0501.2010.02076.x
50. Naitoh M, Hirukawa A, Katsumata A, Ariji E. Evaluation of voxel values in mandibular cancellous bone: relationship between cone-beam computed tomography and multislice helical computed tomography. *Clin Oral Implants Res* 2009; **20**: 503–6. doi: 10.1111/j.1600-0501.2008.01672.x
51. Naitoh M, Hirukawa A, Katsumata A, Ariji E. Prospective study to estimate mandibular cancellous bone density using large-volume cone-beam computed tomography. *Clin Oral Implants Res* 2010; **21**: 1309–13. doi: 10.1111/j.1600-0501.2010.01950.x
52. Nishino K, Shimamoto H, Kakimoto N, Tsujimoto T, Chindasombatjaroen J, Murakami S, et al. Influence of an object's z-axis location and location on the axial plane on the voxel value representation and uniformity in cone-beam computed tomography. *Oral Surg Oral Med Oral Pathol Oral Radiol* 2014; **118**: 619–24. doi: 10.1016/j.oooo.2014.08.010
53. Nomura Y, Watanabe H, Honda E, Kurabayashi T. Reliability of voxel values from cone-beam computed tomography for dental use in evaluating bone mineral density. *Clin Oral Implants Res* 2010; **21**: 558–62. doi: 10.1111/j.1600-0501.2009.01896.x
54. Nomura Y, Watanabe H, Shirotsu K, Honda E, Sumi Y, Kurabayshi T. Stability of voxel values from cone-beam computed tomography for dental use in evaluating bone mineral content. *Clin Oral Implants Res* 2013; **24**: 543–8. doi: 10.1111/j.1600-0501.2012.02420.x
55. Oliveira ML, Freitas DQ, Ambrosano GM, Haiter-Neto F. Influence of exposure factors on the variability of CBCT voxel values: a phantom study. *Dentomaxillofac Radiol* 2014; **43**: 20140128. doi: 10.1259/dmfr.20140128
56. Parsa A, Ibrahim N, Hassan B, Motroni A, van der Stelt P, Wismeijer D. Reliability of voxel gray values in cone beam computed tomography for preoperative implant planning assessment. *Int J Oral Maxillofac Implants* 2012; **27**: 1438–42.
57. Parsa A, Ibrahim N, Hassan B, van der Stelt P, Wismeijer D. Bone quality evaluation at dental implant site using multislice CT, micro-CT, and cone beam CT. *Clin Oral Implants Res* Dec 2013. Epub ahead of print. doi: 10.1111/clr.12315
58. Parsa A, Ibrahim N, Hassan B, Motroni A, van der Stelt P, Wismeijer D. Influence of cone beam CT scanning parameters on grey value measurements at an implant site. *Dentomaxillofac Radiol* 2013; **42**: 79884780. doi: 10.1259/dmfr/79884780
59. Pauwels R, Stamatakis H, Manousaridis G, Walker A, Michielsen K, Bosmans H, et al. Development and applicability of a quality control phantom for dental cone-beam CT. *J Appl Clin Med Phys* 2011; **12**: 3478. doi: 10.1120/jacmp.v12i4.3478
60. Pauwels R, Nackaerts O, Bellaiche N, Stamatakis H, Tsiklakis K, Walker A, et al. Variability of dental cone beam CT grey values for density estimations. *Br J Radiol* 2013; **86**: 20120135. doi: 10.1259/bjr.20120135
61. Plachtovics M, Bujtar P, Nagy K, Mommaerts M. High-quality image acquisition by double exposure overlap in dental cone beam computed tomography. *Oral Surg Oral Med Oral Pathol Oral Radiol* 2014; **117**: 760–7. doi: 10.1016/j.oooo.2014.02.024
62. Reeves TE, Mah P, McDavid WD. Deriving Hounsfield units using grey levels in cone beam CT: a clinical application. *Dentomaxillofac Radiol* 2012; **41**: 500–8. doi: 10.1259/dmfr/31640433
63. Sennerby L, Andersson P, Pagliani L, Giani C, Moretti G, Molinari M, et al. Evaluation of a novel cone beam computed tomography scanner for bone density examinations in preoperative 3D reconstructions and correlation with primary implant stability. *Clin Implant Dent Relat Res* Dec 2013. Epub ahead of print. doi: 10.1111/cid.12193
64. Silva IM, Freitas DQ, Ambrosano GM, Bóscolo FN, Almeida SM. Bone density: comparative evaluation of Hounsfield units in multislice and cone-beam computed tomography. *Braz Oral Res* 2012; **26**: 550–6.
65. Spin-Neto R, Gotfredsen E, Wenzel A. Variation in voxel value distribution and effect of time between exposures in six CBCT units. *Dentomaxillofac Radiol* 2014; **43**: 20130376. doi: 10.1259/dmfr.20130376
66. Valiyaparambil JV, Yamany I, Ortiz D, Shafer DM, Pendrys D, Freilich M, et al. Bone quality evaluation: comparison of cone beam computed tomography and subjective surgical assessment. *Int J Oral Maxillofac Implants* 2012; **27**: 1271–7.
67. Yamashina A, Tanimoto K, Sutthiprapaporn P, Hayakawa Y. The reliability of computed tomography (CT) values and dimensional measurements of the oropharyngeal region using cone beam CT: comparison with multidetector CT. *Dentomaxillofac Radiol* 2008; **37**: 245–51. doi: 10.1259/dmfr/45926904
68. Barone A, Covani U, Cornelini R, Gherlone E. Radiographic bone density around immediately loaded oral implants. *Clin Oral Implants Res* 2003; **14**: 610–15.
69. Brosh T, Yekaterina BE, Pilo R, Shpack N, Geron S. Can cone beam CT predict the hardness of interradicular cortical bone? *Head Face Med* 2014; **10**: 12. doi: 10.1186/1746-160X-10-12
70. Fuster-Torres MÁ, Peñarrocha-Diago M, Peñarrocha-Oltra D, Peñarrocha-Diago M. Relationships between bone density values from cone beam computed tomography, maximum insertion torque, and resonance frequency analysis at implant

placement: a pilot study. *Int J Oral Maxillofac Implants* 2011; **26**: 1051–6.
71. Kaya S, Yavuz I, Uysal I, Akkus Z. Measuring bone density in healing periapical lesions by using cone beam computed tomography: a clinical investigation. *J Endod* 2012; **38**: 28–31. doi: 10.1016/j.joen.2011.09.032
72. Lee S, Gantes B, Riggs M, Crigger M. Bone density assessments of dental implant sites: 3. Bone quality evaluation during osteotomy and implant placement. *Int J Oral Maxillofac Implants* 2007; **22**: 208–12.
73. Simon JH, Enciso R, Malfaz JM, Roges R, Bailey-Perry M, Patel A. Differential diagnosis of large periapical lesions using cone-beam computed tomography measurements and biopsy. *J Endod* 2006; **32**: 833–7.
74. Song YD, Jun SH, Kwon JJ. Correlation between bone quality evaluated by cone-beam computerized tomography and implant primary stability. *Int J Oral Maxillofac Implants* 2009; **24**: 59–64.
75. Tatli U, Salimov F, Kürkcü M, Akoğlan M, Kurtoğlu C. Does cone beam computed tomography-derived bone density give predictable data about stability changes of immediately loaded implants?: a 1-year resonance frequency follow-up study. *J Craniofac Surg* 2014; **25**: e293–9. doi: 10.1097/SCS.0000000000000727
76. Tyndall DA, Price JB, Tetradis S, Ganz SD, Hildebolt C, Scarfe WC; American Academy of Oral and Maxillofacial Radiology. Position statement of the American Academy of Oral and Maxillofacial Radiology on selection criteria for the use of radiology in dental implantology with emphasis on cone beam computed tomography. *Oral Surg Oral Med Oral Pathol Oral Radiol* 2012; **113**: 817–26. doi: 10.1016/j.oooo.2012.03.005
77. Harris D, Horner K, Gröndahl K, Jacobs R, Helmrot E, Benic GI, et al. E.A.O. guidelines for the use of diagnostic imaging in implant dentistry 2011. A consensus workshop organized by the European Association for Osseointegration at the Medical University of Warsaw. *Clin Oral Implants Res* 2012; **23**: 1243–53. doi: 10.1111/j.1600-0501.2012.02441.x
78. European Commission. Cone beam CT for dental and maxillofacial radiology: evidence based guidelines, radiation protection publication 172. Luxembourg: European Commission; 2012.
79. American Association of Endodontists; American Academy of Oral and Maxillofacial Radiology. Use of cone-beam computed tomography in endodontics Joint Position Statement of the American Association of Endodontists and the American Academy of Oral and Maxillofacial Radiology. *Oral Surg Oral Med Oral Pathol Oral Radiol Endod* 2011; **111**: 234–7. doi: 10.1016/j.tripleo.2010.11.012
80. European Society of Endodontology; Patel S, Durack C, Abella F, Roig M, Shemesh H, Lambrechts P, et al. European Society of Endodontology position statement: the use of CBCT in endodontics. *Int Endod J* 2014; **47**: 502–4. doi: 10.1111/iej.12267
81. Pauwels R, Beinsberger J, Collaert B, Theodorakou C, Rogers J, Walker A, et al. Effective dose range for dental cone beam computed tomography scanners. *Eur J Radiol* 2012; **81**: 267–71. doi: 10.1016/j.ejrad.2010.11.028
82. Lettry S, Seedhom BB, Berry E, Cuppone M. Quality assessment of the cortical bone of the human mandible. *Bone* 2003; **32**: 35–44.
83. Viberg B, Ryg J, Overgaard S, Lauritsen J, Ovesen O. Low bone mineral density is not related to failure in femoral neck fracture patients treated with internal fixation. *Acta Orthop* 2014; **85**: 60–5. doi: 10.3109/17453674.2013.875360
84. Fazzalari NL, Parkinson IH. Fractal dimension and architecture of trabecular bone. *J Pathol* 1996; **178**: 100–5.
85. Hua Y, Nackaerts O, Duyck J, Maes F, Jacobs R. Bone quality assessment based on cone beam computed tomography imaging. *Clin Oral Implants Res* 2009; **20**: 767–71. doi: 10.1111/j.1600-0501.2008.01677.x
86. González-Martín O, Lee EA, Veltri M. CBCT fractal dimension changes at the apex of immediate implants placed using undersized drilling. *Clin Oral Implants Res* 2012; **23**: 954–7.
87. Huang Y, Van Dessel J, Liang X, Depypere M, Zhong W, Ma G, et al. Effects of immediate and delayed loading on peri-implant trabecular structures: a cone beam CT evaluation. *Clin Implant Dent Relat Res* Apr 2013. Epub ahead of print. doi: 10.1111/cid.12063
88. Torres SR, Chen CS, Leroux BG, Lee PP, Hollender LG, Schubert MM. Fractal dimension evaluation of cone beam computed tomography in patients with bisphosphonate-associated osteonecrosis. *Dentomaxillofac Radiol* 2011; **40**: 501–5. doi: 10.1259/dmfr/14636637
89. Lee TC, Kashyap RL, Chu CN. Building skeleton models via 3-D medial surface axis thinning algorithms. *CVGIP: Graph Model Image Process* 1994; **56**: 462–78.
90. Odgaard A, Gundersen HJG. Quantification of connectivity in cancellous bone, with special emphasis on 3-D reconstructions. *Bone* 1993; **14**: 173–82.
91. Hildebrand T, Rüegsegger P. A new method for the model-independent assessment of thickness in three-dimensional images. *J Microsc* 1997; **185**: 67–75.
92. Hildebrand T, Rüegsegger P. Quantification of bone microarchitecture with the structure model index. *Comput Methods Biomech Biomed Engin* 1997; **1**: 15–23.
93. Van Dessel J, Huang Y, Depypere M, Rubira-Bullen I, Maes F, Jacobs R. A comparative evaluation of cone beam CT and micro-CT on trabecular bone structures in the human mandible. *Dentomaxillofac Radiol* 2013; **42**: 20130145. doi: 10.1259/dmfr.20130145
94. González-García R, Monje F. The reliability of cone-beam computed tomography to assess bone density at dental implant recipient sites: a histomorphometric analysis by micro-CT. *Clin Oral Implants Res* 2013; **24**: 871–9. doi: 10.1111/j.1600-0501.2011.02390.x
95. Hsu JT, Wang SP, Huang HL, Chen YJ, Wu J, Tsai MT. The assessment of trabecular bone parameters and cortical bone strength: a comparison of micro-CT and dental cone-beam CT. *J Biomech* 2013; **46**: 2611–18. doi: 10.1016/j.jbiomech.2013.08.004
96. Ibrahim N, Parsa A, Hassan B, van der Stelt P, Aartman IH, Nambiar P. Influence of object location in different FOVs on trabecular bone microstructure measurements of human mandible: a cone beam CT study. *Dentomaxillofac Radiol* 2014; **43**: 20130329. doi: 10.1259/dmfr.20130329
97. Ibrahim N, Parsa A, Hassan B, van der Stelt P, Aartman IH, Wismeijer D. The effect of scan parameters on cone beam CT trabecular bone microstructural measurements of human mandible. *Dentomaxillofac Radiol* 2013; **42**: 20130206.